

## Implications of a Pressure Induced Phase Transition in the Search for Cubic Ti<sub>3</sub>Al

P. Ch. Sahu, N. V. Chandra Shekar, Mohammad Yousuf, and K. Govinda Rajan

Materials Science Division, Indira Gandhi Centre for Atomic Research, , Kalpakkam 603102, Tamil Nadu, India  
(Received 31 July 1996)

High-pressure x-ray diffraction studies of the high temperature structural intermetallic, Ti<sub>3</sub>Al (*DO*<sub>19</sub> structure at NTP), were carried out with the motivation of finding clues for identifying the alloying elements for stabilizing the cubic *L*<sub>12</sub> structure, which is expected to have better ductility. The present investigation revealed a structural transition from *DO*<sub>19</sub> to *DO*<sub>24</sub> structure in the pressure range 10–15 GPa. The geometrical relationship between these two structures and the possible mechanism of the transition have been elucidated. From this investigation follow two important results that may have significant bearing in the search for the cubic Ti<sub>3</sub>Al. [S0031-9007(97)02317-X]

PACS numbers: 61.66.Fn, 62.50.+p, 64.70.Kb, 81.40.Vw

The high temperature structural intermetallic Ti<sub>3</sub>Al has attractive properties which make it a favorable candidate for applications in the aerospace industry. The primary advantages of Ti<sub>3</sub>Al are its high specific strength at elevated temperatures, high melting temperature, and excellent environmental and creep resistance properties [1,2]. However, it has a serious drawback of poor ductility resulting in low fracture toughness and fast fatigue crack growth [2]. The ductility of a material depends on several factors, but in Ti<sub>3</sub>Al, it has been mainly attributed to the hexagonal *DO*<sub>19</sub> (Ni<sub>3</sub>Sn type) crystal structure with a limited number of active slip systems [3,4] and directional (covalent) bonding between the constituent ions with anisotropic charge distributions [5,6]. In *DO*<sub>19</sub> structure, five independent slip systems are possible [7], which would satisfy the Von Mises criterion for uniform deformation [8]. But in Ti<sub>3</sub>Al, the yield stresses for different slip systems are widely different [9], and thus not all the five slip systems are activated during deformation, leading to cleavage fracture [10]. Single crystals of Ni<sub>3</sub>Al and Zr<sub>3</sub>Al, with high symmetry cubic *L*<sub>12</sub> structure, having enough number of active slip systems satisfying the Von Mises criterion, are quite ductile [4,6].

It is always possible to improve the ductility and strength of a binary alloy by stabilizing the high symmetry cubic phase with the desired electronic structure by a suitable ternary addition [7,10]. But the problem lies in choosing the appropriate alloying elements. Tremendous efforts have been made to improve the ductility and strength of Ti<sub>3</sub>Al through the various possible routes, but it has not become successful so far [11]. Guided by Pettifor's phenomenological *AB*<sub>3</sub> structural map, the attempts made in this direction by alloying with some rare-earth elements also have failed [3]. Some electronic structure and comparative structural stability calculations between the *DO*<sub>19</sub> and the *L*<sub>12</sub> structure have been made [12,13], but the major drawback in all these calculations lies in the assumption that there are no other structural transitions in between these two structures! Based on these types of calculations [13], a phase transition to the *L*<sub>12</sub> structure has been predicted at about 25 GPa. The role of high pressure in

selecting the alloying elements to modify the crystal and physical properties is well known [14]. But surprisingly, no such efforts have been reported to date. The present high pressure investigation on Ti<sub>3</sub>Al was taken up to study its structural stability behavior which may provide valuable clues in this direction.

The Ti<sub>3</sub>Al samples were prepared by arc melting the stoichiometric quantities of Ti (99.9% pure) and Al (99.999% pure) in an inert environment. The melted ingots were vacuum sealed in silica tubes and were annealed at a temperature of ~1200 K for six weeks. The annealed ingots were powdered and characterized by x-ray diffraction (XRD) using a Guinier diffractometer described elsewhere [15]. The sample was found to be in single phase and the lattice parameters obtained were  $a = 5.818(2) \text{ \AA}$ ,  $c = 4.689(2) \text{ \AA}$ , and  $c/a = 0.806$  (with the number of molecules in the unit cell,  $Z = 2$ ) which are very close to the standard JCPDS values.

Finely powdered Ti<sub>3</sub>Al sample mixed with a small quantity of Ag was loaded into the stainless steel gasket hole of diameter 250  $\mu\text{m}$  (the diamond anvil culet diameter was 500  $\mu\text{m}$ ). A mixture of methanol, ethanol, and water in the ratio 16:3:1 was used as the pressure transmitting fluid which ensures hydrostatic pressure up to ~20 GPa. The equation of state (EOS) of Ag was used as the internal pressure standard. High-pressure x-ray diffraction (HPXRD) was carried out in the angle dispersive mode by using a Mao-Bell-type DAC and a novel Guinier diffractometer described in Ref. [15]. The incident Mo x ray, obtained from a Rigaku 18 kW rotating anode x-ray generator, was monochromatized by a curved quartz crystal monochromator and an almost pure  $K_{\alpha 1}$  beam was impinged on the sample. A flat position sensitive detector (PSD) was used for detecting the diffracted x rays. A PSD scan time of 2 h was required for acquiring each HPXRD spectrum. The experiments were performed up to a maximum pressure of ~41 GPa.

The high-pressure x-ray diffraction spectra were analyzed by the standard techniques and the *P-V* data of Ti<sub>3</sub>Al up to ~41 GPa are shown in Fig. 1. After an initial normal compression up to ~10 GPa, it showed a structural phase

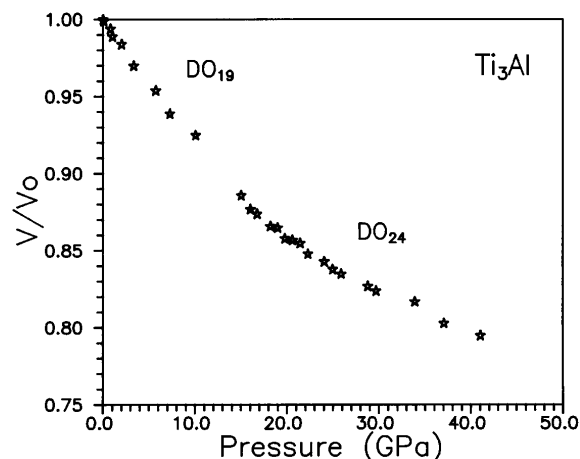


FIG. 1.  $P$ - $V$  data for  $\text{Ti}_3\text{Al}$  up to  $\sim 41$  GPa. The  $P$ - $V$  data are not shown in the transition zone, 10–15 GPa.

transition in the pressure range 10–15 GPa with a small volume change of  $\sim 1\%$ . This transition was reversible in nature with a hysteresis of  $\sim 6$  GPa. The  $P$ - $V$  data up to 10 GPa were fitted to both the Birch-Murnaghan and Vinet EOS [16,17] to obtain the bulk modulus  $B_0$  and its pressure derivative  $B'_0$ . The  $B_0$  and the  $B'_0$  values obtained in this study are  $106.7 \pm 5.8$  GPa and  $3.7 \pm 1.5$  with the Birch-Murnaghan EOS, and  $106.7 \pm 5.9$  GPa and  $3.7 \pm 1.6$  with the Vinet EOS, respectively. The  $P$ - $V$  data for the high-pressure phase were also fitted to the above EOS in their modified forms [18].  $P = P_r + f(V/V_r)$ . Here  $V$  and  $V_r$  are the volumes at pressures  $P$  and  $P_r$ , respectively.  $P_r$  was fixed at 15 GPa, the pressure above which the second phase existed. The bulk modulus at pressure  $P_r = 15$  GPa and its pressure derivative ( $B_r$  and  $B'_r$ ) obtained by this method for the high-pressure phase are  $136.0 \pm 7.0$  GPa and  $11.7 \pm 1.6$  with the Birch-Murnaghan EOS, and  $139.0 \pm 6.2$  GPa and  $10.4 \pm 1.0$  with the Vinet EOS, respectively.

Indications of the structural phase transition were seen at pressures above  $\sim 10$  GPa with the appearance of a new peak to the right of the 100% (201) peak of the parent  $\text{DO}_{19}$  structure [Fig. 2]. With further increase of pressure, the intensity of the new peak increased and that of the parent (201) peak decreased. Other minor changes in the peak positions and their intensities also can be noticed in Fig. 2. The structural transition was found to be completed at about 15 GPa, above which the relative intensities of the peaks remained almost constant. The transition was not sharp and it had a width of  $\sim 5$  GPa. It may be noted that the hydrostatic limit of pressure in our experiment is up to  $\sim 20$  GPa and the large width of this transition cannot be attributed to the nonhydrostatic pressure medium. We believe this to be due to the inherent sluggish nature of the transition.

The structure of the high-pressure phase was identified to be  $\text{DO}_{24}$  ( $\text{Ni}_3\text{Ti}$  type) with the lattice parameters

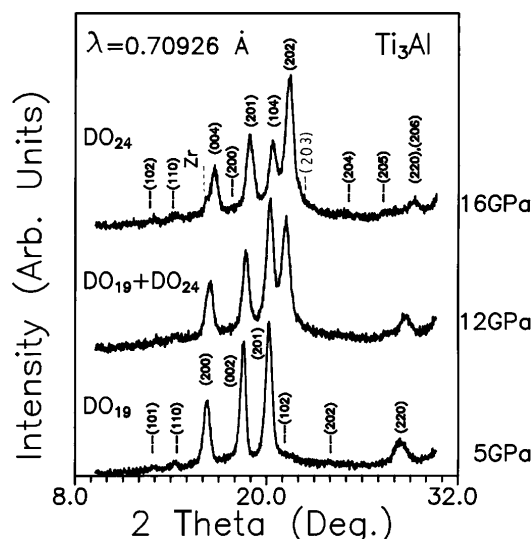


FIG. 2. High-pressure x-ray diffraction patterns of  $\text{Ti}_3\text{Al}$  obtained with the PSD and the Guinier diffractometer at 5 GPa, 12 GPa, and 16 GPa. The appearance of a new peak to the right of the parent (201) peak (middle spectrum) and the gradual increase in the intensity at the expense of the parent (201) peak can be noticed (top spectrum). Small changes in the positions and intensities of the other peaks also can be noticed. The shoulder to the left of the (004) peak is due to the projection of the Zr shim (placed between the cylinder diamond and the tungsten carbide rocker) into the x-ray path. The high pressure phase is indexed to the  $\text{DO}_{24}$  structure.

$a = 5.312(10)$  Å,  $c = 9.604(10)$  Å,  $c/a = 1.808$ , and  $Z = 4$  corresponding to a pressure of  $\sim 16$  GPa. The observed and calculated  $d$  spacings and intensities are shown in Table I. The observed  $d$  spacings of all the

TABLE I. The observed and calculated  $d$  spacings and intensities ( $I$ ) for the diffraction peaks of the  $\text{DO}_{24}$  structure at  $P = 16$  GPa.

Peak No.	$d$ (obs.) (Å)	$d$ (Cal.) (Å)	$I$ (obs.) (%)	$I$ (Cal.) (%)	$hkl$
1	3.337	3.3221	5	5.3	102
2	2.664	2.6563	5	2.7	110
3	2.413	2.4010	35	45.5	004
4	2.295	2.3004	5	7.5	200
5	2.228	2.2371	50	41.7	201
6	2.126	2.1286	35	0.2	104
7	2.077	2.0746	100	100	202
8	1.870	1.8681	4	24.1	203
9	1.655	1.6611	5	5.5	204
10	1.471	1.4744	4	11.0	205
11	1.327	1.3281	15	20.2	220,
		1.3139		22.0	206
12	1.199	1.2005	7	4.6	008
13	1.179	1.1783	5	5.1	207
14	1.163	1.1622	15	24.4	224
15	1.119	1.1186	7	11.8	402
16	1.084	1.0824	5	3.5	403

reflections match reasonably well with the calculated values. However, the same is not true for the intensities. But in HPXRD experiments, the intensity matching is an inherent and well known problem and is attributed mainly to preferred orientation of the sample particles in the DAC. The space group of this new structure is the same as that of the parent phase (space group  $P6_3/mmc$ ), but with an almost twice  $c/a$  ratio.

The unit cells of these two structures with the atom positions are shown in Fig. 3. Both the structures are made up of identical  $A_3B$ , ( $A = \text{Ti}, B = \text{Al}$ ) layers of atoms, in which each Al atom is surrounded by 6 Ti atoms. The  $DO_{19}$  structure is obtained by  $AB$  stacking of these layers, whereas the  $DO_{24}$  structure with  $ABAC$  stacking. By the application of pressure, the  $DO_{24}$  structure can evolve from the  $DO_{19}$  structure with the movement of the successive atomic layers by a distance  $a/2$  with respect to the basal plane (0001) either in the  $\langle 10\bar{1}0 \rangle$  or the  $\langle 11\bar{2}0 \rangle$  directions. This mechanism appears to be convincing from the fact that the yield stresses for these basal slips are minimum compared to the other slip systems [9]. In this process the  $z = \frac{1}{2}$  atomic layers in the successive unit cells of the  $DO_{19}$  structure become nonequivalent (Fig. 3), leading to doubling of the unit cell in the  $c$  direction and resulting in the  $DO_{24}$  structure.

The  $DO_{24}$  structure observed in this investigation has never been encountered earlier in the realm of Ti-Al intermetallics. The structures mostly observed or discussed in literature are the  $L1_0$ ,  $L1_2$ ,  $DO_a$ ,  $DO_{19}$ ,  $DO_{22}$ ,

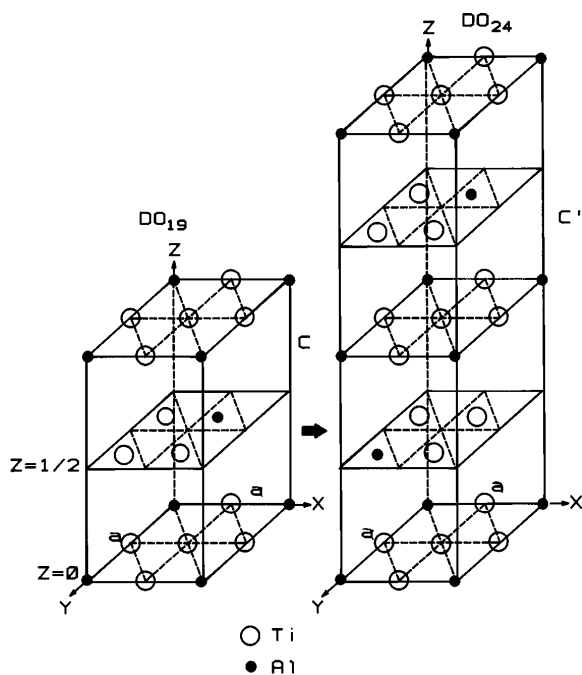


FIG. 3. The unit cells of the  $DO_{19}$  and  $DO_{24}$  structures with the atom positions indicated. The relation between these two structures and the possible mechanism of the transition has been explained in the text.

$DO_{23}$ ,  $DO_{25}$ , etc. In the  $DO_{19}$  structure, the cubic environment of the atoms is zero, whereas that in the  $DO_{24}$  structure is 50%. It appears that it may eventually transform to the  $L1_2$  structure with 100% cubic environment of atoms at higher pressures. Such a structural sequence ( $DO_{19}$ - $DO_{24}$ - $L1_2$ ) with increasing cubic environment of atoms has been seen in the rare-earth trialuminides,  $RA\text{Al}_3$  ( $R = \text{La}-\text{Yb}$ ), as a function of increasing atomic number or decreasing atomic radii of the rare-earth elements [19]. The actual structural sequence observed is  $DO_{19}$  (0%)- $\text{BaPb}_3$  type (33%)- $DO_{24}$  (50%)- $\text{HoAl}_3$  (60%)- $L1_2$  (100%) with two more intermediate structures. The numbers in the brackets indicate the percentage of the cubic environment of atoms. The same structural sequence has been observed in these rare-earth trialuminides as a function of pressure [20]. The present investigation thus seems to indicate that  $\text{Ti}_3\text{Al}$  is also following the similar structural sequence as the rare-earth trialuminides under pressure.

From the above discussion, two important results follow which will have significant bearing in the search for the pseudobinary cubic  $\text{Ti}_3\text{Al}$ . The first one is regarding the possible intermediate phases the system may adopt before transforming to the cubic  $L1_2$  phase from the initial  $DO_{19}$  phase. In the earlier structural stability calculations [12,13], no intermediate structures between the  $DO_{19}$  and the  $L1_2$  structures have been taken into consideration. Hence it is not surprising that the prediction of a phase transition based on such calculations was not observed. But the present investigation clearly suggests the possible intermediate structures ( $\text{BaPb}_3$ - $DO_{24}$ - $\text{HoAl}_3$ ) to be considered for structural stability calculations. This may evoke a renewed interest in electronic structure and structural stability calculations in  $\text{Ti}_3\text{Al}$  with the objective of solving this long standing problem.

The second important result follows from the fact that under pressure,  $\text{Ti}_3\text{Al}$  also seems to be following the similar structural sequence ( $DO_{19}$ - $DO_{24}$ - $L1_2$ ) as in the rare-earth trialuminides as a function of decreasing atomic radii of the rare-earth elements or increasing pressure. This implies that for stabilizing  $\text{Ti}_3\text{Al}$  in the  $L1_2$  structure, one should choose an alloying element whose atomic radius is smaller than that of Ti. This may be contrasted with the earlier unsuccessful attempts [3] guided by Pettifor's two dimensional structural maps. In these studies the alloying elements chosen were the rare-earths like Y, Er, and Sc whose atomic radii are higher than that of Ti. This shows the inadequacy of the use of the structural maps in their predictive mode. Strong support from electronic structure calculations is essential for making these types of attempts successful. In the present investigation, although it is suggested that the alloying elements should be of smaller sizes compared to Ti, further electronic structure calculations are essential to arrive at the exact alloying element which will not only stabilize  $\text{Ti}_3\text{Al}$  in the cubic  $L1_2$  phase, but also ensure a

symmetric charge distribution around the constituent ions for better ductility and strength.

The above two important results are expected to evoke fresh interest in  $Ti_3Al$  among both the theoretical and experimental alloy designers. This may also motivate the high pressure investigators to initiate work on systems whose physical properties and the crystal structures are to be tailored in the desired direction.

In summary, high-pressure structural investigation on  $Ti_3Al$  was carried out up to  $\sim 41$  GPa. A structural phase transition from the  $DO_{19}$  to the  $DO_{24}$  structure was observed in the pressure range 10–15 GPa. By drawing an analogy with the rare-earth trialuminides, it is predicted that it may eventually transform to the cubic  $L1_2$  structure at still higher pressure. For structural stability calculations, the possible intermediate structures to be considered between the  $DO_{19}$  and the  $L1_2$  structures are identified. For stabilizing  $Ti_3Al$  in the cubic phase, the atomic radius of the alloying element should be smaller than that of Ti. The reasons for the failure of such earlier attempts guided by the structural maps were attributed to the higher atomic radii of the alloying elements. Electronic structure calculations are essential to reinforce the findings from the structural maps and experimental investigations in the game of designing structural alloys.

The authors thank Mr. L. Meenakshi Sundaram for his help in preparing the  $Ti_3Al$  sample; Mr. N. Subramanian, Mr. M. Sekar, and Ms. S. Sarojini for their help at various stages of this work and useful discussions; and Dr. R. Asokamani for bringing this problem to our notice. They thank Dr. T. S. Radhakrishnan, Dr. Kanwar Krishan, Dr. Baldev Raj, and Dr. Placid Rodriguez for their encouragement and support.

- [1] G. Sauthoff, in *Materials Science and Technology*, edited by R. W. Cahn, P. Haasen, and E. J. Kramer (VCH, Weinheim, 1996), Vol. 8, p. 643.
- [2] H. A. Lipsitt, *Mater. Res. Soc. Symp. Proc.* **39**, 351 (1985).
- [3] C. T. Liu, J. A. Horton, and D. G. Pettifor, *Mater. Res. Soc. Symp. Proc.* **133**, 37 (1989).
- [4] M. Yamaguchi and Y. Umakoshi, *Prog. Mater. Sci.* **34**, 1 (1990).
- [5] C. L. Fu, *J. Mater. Res.* **5**, 971 (1990).
- [6] M. E. Eberhart, D. P. Clougherty, and J. M. Maclaren, *J. Mater. Res.* **8**, 438 (1993).
- [7] C. T. Liu and J. O. Stiegler, *Science* **226**, 636 (1984).
- [8] R. Von Mises, *Z. Angew. Math. Mech.* **8**, 161 (1928).
- [9] T. Nakano and Y. Umakoshi, *J. Alloys Compd.* **197**, 17 (1993).
- [10] F. H. Froes, C. Suryanarayana, and D. Eliezer, *Trans. Iron Steel Inst. Jpn.* **31**, 1235 (1991).
- [11] J. J. Davies and A. A. Ogwu, *J. Alloys Compd.* **228**, 105 (1995).
- [12] T. Hong, J. M. Watson-Yang, X. Q. Guo, A. J. Freeman, and T. Oguchi, *Phys. Rev. B* **43**, 1940 (1991).
- [13] P. Ravindran and R. Asokamani, *Phys. Rev. B* **50**, 668 (1994).
- [14] A. Jayaraman, *Met. Mater. Processes* **2**, 1 (1990).
- [15] P. Ch. Sahu, Mohammad Yousuf, N. V. Chandra Shekar, N. Subramanian, and K. Govinda Rajan, *Rev. Sci. Instrum.* **66**, 295 (1995).
- [16] F. Birch, *J. Geophys. Res.* **57**, 227 (1962).
- [17] P. Vinet, J. Ferrante, J. H. Rose, and J. R. Smith, *J. Geophys. Res.* **92**, 9319 (1987).
- [18] W. A. Grosshans and W. B. Holzapfel, *Phys. Rev. B* **45**, 5179 (1992).
- [19] J. H. N. Van Vucht and K. H. J. Buschow, *J. Less-Common Met.* **10**, 98 (1965); J. H. N. Van Vucht, *J. Less-Common Met.* **11**, 308 (1966).
- [20] J. F. Cannon and H. T. Hall, *J. Less-Common Met.* **40**, 313 (1975).